Journal of Power Sources 196 (2011) 5951–5959

Contents lists available at ScienceDirect

Journal of Power Sources

journal homepage: www.elsevier.com/locate/jpowsour

Understanding the sucrose-assisted combustion method: Effects of the atmosphere and fuel amount on the synthesis and electrochemical performances of $LiNi_{0.5}Mn_{1.5}O_4$ spinel

José Manuel Amarilla*, Rosa M. Rojas, José María Rojo

Instituto de Ciencia de Materiales de Madrid, Consejo Superior de Investigaciones Científicas (CSIC), Sor Juana Inés de la Cruz 3, 28049 Madrid, Spain

ARTICLE INFO

Article history:
Received 3 December 2010
Received in revised form 15 February 2011
Accepted 27 February 2011
Available online 6 March 2011

Keywords:
Lithium battery
Combustion synthesis
$LiNi_{0.5}Mn_{1.5}O_4$
5 V-cathode
Spinel
Mass spectrometry

ABSTRACT

The present paper comprises results of our studies about the influence of the atmosphere and fuel amount on the synthesis and electrochemical performance of $LiNi_{0.5}Mn_{1.5}O_4$ spinel (LNMS). Reaction of mixtures of metal nitrates with and without sucrose (fuel) in Ar and in air flow has been studied by thermal analysis and coupled mass spectrometry (TG/DTA/MS). Products obtained after the thermal study have been identified and characterized by powder X-ray diffraction (XRD) and field emission scanning electron microscopy (FE-SEM). Gases evolved along the thermal treatment have been identified by coupled mass spectrometry (MS). From all these results the synthesis reactions have been put forward. When the reaction is conducted in air sub-micrometric $LiNi_{0.5}Mn_{1.5}O_4$ spinel is obtained independently of the amount of sucrose. When the reaction is done in Ar the spinel is only obtained in absence of fuel. The electrochemical performances at 25 °C and 55 °C of the synthesized LNMSs have been evaluated by galvanostatic cycling. The samples prepared in air furnish high capacity (≈120 mAh g^{-1}) and they work at high voltage (≈4.7 V). Besides, they exhibit remarkable cycling properties, even at elevated temperature (55 °C), with capacity retentions higher than 90% after 50 cycles.

1. Introduction

Solution or low temperature combustion synthesis (LCS) is a synthesis procedure based on an oxidation–reduction reaction between soluble precursor salts (oxidizers) and sacrificial, most often carbonaceous, compounds (fuels). Briefly, the LCS consists of bringing a saturated aqueous solution of the metal salts and the fuel to dryness until the mixture ignites and a fast combustion reaction occurs. Owing to fast evaporation of the solvent and release of large volume of thermolytic gaseous products, it results in obtaining a voluminous porous product. The product consists of loosely packed homogeneous crystallites with uniform, usually nanometric particle size. Since the first reports about the synthesis of chromites and perovskites with tetraformal triazine (TFTA), maleic hydrazide or carbohydrazide [1–3], the method has been used for synthesizing many different nanopowder materials [4] compounds such as oxides [5–8], nanophosphors [9–12], using urea [7,8,11,12], sucrose [5], glucose [9], citric acid [6], glycine [10], among others, as fuel. In fact, LCS is a very outstanding synthesis procedure attracting a good deal of attention because it is time and energy saving, and requires simple equipment and cheap reagents.

Li-ion batteries (LIBs) are the state of the art of advanced batteries [13,14]. They are the technology of choice for portable electronic devices and they will be applied to power the next generation of hybrid and battery electrical cars (EVs). In recent years, combustion synthesis is being widely used to prepare electrochemically active materials for LIBs batteries [15–18]. Among the large number of positive electrode (cathode) materials studied, $LiMn_2O_4$-based spinels are one of the best candidates as cathodes for the large-size LIBs needed in EVs [19,20]. In previous papers we have shown that the sucrose-aided LCS constitutes a straightforward and non-expensive method to synthesize nanosized $LiMn_2O_4$-based spinels with many different compositions [21,22]. It has been successfully applied for the synthesis of many cathode materials working in the 4 V and 5 V regions, i.e. low-doped $LiMn_{1.99-y}Li_yM_{0.01}O_4$ ($M = Al^{3+}$, Ni^{2+}, Cr^{3+}, Co^{3+}; $y = 0.01$ and 0.06) [23] and $LiNi_{0.5}Mn_{1.5}O_4$ [24], respectively. The $LiNi_{0.5}Mn_{1.5}O_4$ spinel (hereafter named as LNMS), is one of the cathode materials most intensively studied [25–29] since Zhong et al. [30] showed that it was able to de-/inserted Li^+ ions at very high potential (≈4.7 V vs. Li^+/Li). Besides, it has large reversible capacity (≈130 mAh g^{-1}) and LNMS spinel is able to store high practical specific energy (≈610 mWh g^{-1}), even higher than $LiFePO_4$, $LiMn_2O_4$ and $LiCoO_2$. We have considered worthwhile to deepen the knowledge of the reactions taking place during synthesis of the $LiMn_2O_4$-based spinels by the sucrose-assisted LCS. To achieve this goal, and because of their remarkable electrochem-

* Corresponding author. Tel.: +34 91 334 90 74; fax: +34 91 372 06 23.
E-mail address: amarilla@icmm.csic.es (J.M. Amarilla).

0378-7753/$ – see front matter © 2011 Elsevier B.V. All rights reserved.
doi:10.1016/j.jpowsour.2011.02.084

ical performances, the synthesis of the $LiNi_{0.5}Mn_{1.5}O_4$ spinel has been studied. The proposed reaction to describe the synthesis of the LNMS-spinel by the sucrose-assisted LCS in a closed system is:

$$LiNO_3 + 0.5Ni(NO_3)_2 + 1.5Mn(NO_3)_2 + wC_{12}H_{22}O_{11} \rightarrow LiMn_{1.5}Ni_{0.5}O_4 + \text{gases evolved} \quad (1)$$

The oxidizing valence of $LiNO_3$ is 5, that of both the $Ni(NO_3)_2$ and $Mn(NO_3)_2$ is 10, whereas the reducing valence of the sucrose is 48 [3]. Based on the thermochemical parameters of the fuel-oxidizer mixtures used in the propellants field, the ratio of oxidizing and reducing valences should be unity [3]. It implies that the ratio of total metal nitrates to fuel in Eq. (1) should be $w = 0.52$ mol. Therefore, the stoichiometric amount required for the synthesis of the $LiMn_{1.5}Ni_{0.5}O_4$ spinel would be ≈0.5 mol of sucrose. However, we had observed that when this amount of sucrose is used, the reaction was very violent. If the amount of sucrose was twice the stoichiometric one, i.e. 1 mol, the reaction was not as violent and the yield of the reaction was very high (≈96%) [24]. These results demonstrate that the amount of fuel plays a major role in the sucrose-assisted LCS procedure.

According to Eq. (1), the auto-combustion process that allows the synthesis of the LNMS should be a redox type of reaction, in which nitrate ions act as oxidant and sucrose acts as fuel. From this reaction, oxygen could be generated in situ resulting in the oxidation of the Mn^{2+} so that no extra oxygen out of the reagents should be necessary. To investigate this assumption we have undertaken the study of the thermal behavior of the mixture of reagents, nitrates and sucrose, in inert and in air atmosphere; i.e. we have study the influence of the atmosphere on the mechanism of the sucrose-assisted combustion synthesis. Additionally, we have also examined the reactions when two different amounts of sucrose (fuel), 0.5 mol and 1 mol, are used for the synthesis of the LNMS. The present paper comprises the results of our experimental studies on the sucrose-assisted LCS performed by thermal analysis and coupled-mass spectrometry (TG/DTA/MS), X-ray powder diffraction (XRD) and field emission-scanning electron microscopy (FE-SEM). Results have been compared with those obtained from thermal treatment of the oxidizing nitrate reagents only. Owing to the high technological interest of the $LiNi_{0.5}Mn_{1.5}O_4$-based cathodes, and bearing in mind the TG/DTA/MS results, we have synthesized several LNMS samples in inert atmosphere and in air using different amounts of sucrose. Their electrochemical performances at 25 °C and 55 °C have been determined.

2. Experimental

2.1. Synthesis

Reagent grade $LiNO_3$, $Ni(NO_3)_2{\cdot}4H_2O$ and $Mn(NO_3)_2{\cdot}6H_2O$ in molar ratio 1:0.5:1.5 were grounded together in agate mortar and left overnight in a closed glass bottle. This sample will be hereafter referred as 0S. Mixtures of the same nitrate reagents in the same molar ratios than before were grounded together with 1 and 0.5 mol sucrose $C_{12}H_{22}O_{11}$ in agate mortar, and also left overnight in a closed glass bottle at room temperature. These samples containing 1 and 0.5 mol sucrose, hereafter referred as 1S and 0.5S, respectively, adopted the aspect of a green syrup, while the one that does not contain sucrose, i.e. the sample 0S, was a sticky green mass. The reagent mixtures were then transferred to platinum crucibles and left overnight at 80 °C. After this treatment, samples 1S and 0.5S were brown powders, while sample 0S was a sticky black mass. The so-thermally treated samples were then used in the following X-ray and TG/DTA/MS studies.

2.2. Characterization

The products were characterized with various analytical techniques. X-ray powder diffraction (XRD) patterns were recorded at room temperature, in a Bruker D8 diffractometer, with CuKα radiation, λ = 1.5418 Å. The patterns were obtained in the step scanning mode at 0.02° (2θ) step and 1 s step^{-1} counting time, within the range $10° \leq 2\theta \leq 80°$. Lattice parameters were refined with the CELREF program [31]. The average crystallite size was calculated from several diffraction lines from the Scherrer formula $D = \lambda/\beta\cos\theta$, where λ is the wavelength of CuKα, θ is the diffraction angle, and $\beta = \sqrt{\beta_m^2 - \beta_s^2}$ is the corrected half-width of the diffraction peaks, where β_m is the observed half-width of the experimental diffraction peaks, and β_s is the half-width of the diffraction peaks of a standard sample, in our case an Al_2O_3 flat-plate of the National Institute of Standards Technology (NIST).

Thermal analysis experiments (DTA/TG) were done in a Simultaneous Thermal Analyzer SDT Q600 in Pt crucibles. Analyses were carried out in Argon and in air flow of 200 ml min^{-1} at 10 °C min^{-1} heating rate in the temperature range 25–700 °C. About 10 mg sample was used in each run. Gases evolved (EGA) during the thermal treatments were analyzed by mass spectrometry (MS) with a Pfeiffer ThermoStar™ mass spectrometer coupled to the SDT instrument.

LNMS-samples for electrochemical studies (about 1 g) were obtained as follows: (i) from the 0S reagents mixture, i.e. without sucrose as fuel, heated at 700 °C in N_2 4 h (hereafter referred as 0S-700N); (ii) from sample (i) heated in air at 800 °C 4 h (labelled as 0S-700N800A); (iii) by direct heating of the 0S reagents mixture in air at 800 °C 4 h (0S-800A); and (iv) by the thermal treatment of the 1S reagents mixture at 800 °C 4 h in air (1S-800A). The reaction mixtures were heated at 2 °C min^{-1} heating/cooling rates either in N_2 flow (100 ml min^{-1}) in a tubular furnace, or in still air in a muffle furnace. The study of the particle size and the morphology of these LNMS-samples was carried out by scanning electron microscopy (FE-SEM) using a field emission FE microscopy model Novasem 230. The samples were sprinkled on a conductive sheet of carbon.

2.3. Electrochemical measurements

The study of the electrochemical properties of these LNMS-spinels was performed in two electrode lithium cells. Positive electrode composites were prepared from the spinel powders (≈20 mg or 72 wt.%), MMM Super P carbon black (17 wt.%) and polyvinylidenefluoride (PVDF, 11 wt.%). The three powder components were suspended in 1-methyl-2-pyrrolidinone as fugitive solvent. Cylindrical pellets (12 mm diameter and ≈0.2 mm thickness) of positive electrode were obtained after cold pressing at 370 MPa. The negative electrode was a lithium foil, which also operates as reference electrode. The electrodes were separated by a Whatman BSF80 paper soaked in the electrolyte, which was a 1 M solution of $LiPF_6$ in ethylene carbonate and dimethyl carbonate (1:1, v/v) as supplied by UBE Europe GmbH. The components were assembled into a Swagelok® cell within an argon glove box in which water content was kept below 1 ppm. Cells were galvanostatically cycled at room temperature in the voltage range of 3.4–5 V at 0.2*C* charge/discharge rates with an Arbin-BT4 battery system (1*C* = 147 mA g^{-1}). Electrochemical impedance spectra of the cells during the cycling at 25 °C were registered with an IM6ex Electrochemical Workstation. The amplitude of ac voltage was 5 mV and the spectra were recorded at a constant potential after the appropriate equilibration. The frequency range was from 100 kHz to 1 Hz.

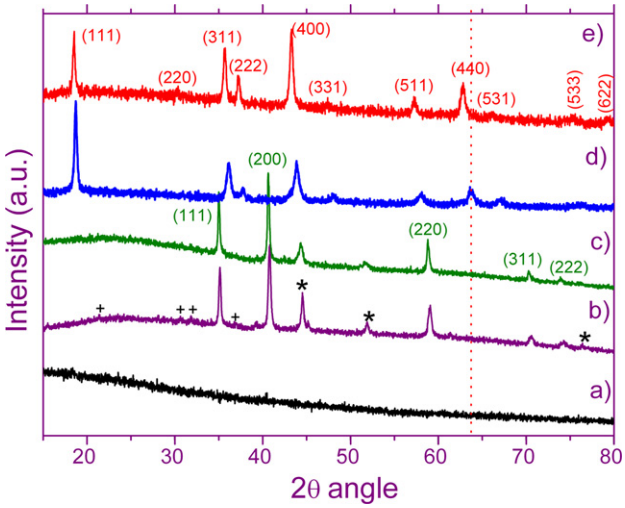

Fig. 1. X-ray diffraction patterns of: (a) reagents mixture of the 1S sample after overnight at 80 °C; (b and c) residues of DTA/TG/MS in Ar flow of samples 1S and 0.5S (indexing corresponds to MnO (78-0424 JCPDS file); peaks marked * and + have been ascribed to NiC (14-002 JCPDS file) and to Li_2CO_3 (83-1454 JCPDS file), respectively; (d) the former residues heated in air at 700 °C; and (e) residue of DTA/TG/MS of sample 0S in Ar flow (indexing correspond to spinel-type structure).

3. Results and discussion

3.1. Thermal, mass spectrometry and X-ray diffraction studies

X-ray powder diffraction patterns recorded for the samples after standing overnight at 80 °C indicated that they were amorphous. In Fig. 1a the XRD pattern of the 1S sample is shown, as an example. TG/DTA/MS analyses were then performed in Ar and in air flow, on these *as-prepared* amorphous precursors. In Fig. 2a, c, and e DTA/TG curves recorded for the 1S, 0.5S and 0S samples in Ar flow are plotted. The corresponding MS are shown in Fig. 2b, d, and f, and the m/z signals identified are gathered in Table 1. Analysis of the DTA/TG curves indicates that on start heating and between room temperature and ≈150 °C the 1S and 0.5S samples undergo a weight loss of ≈10% (Fig. 2a and c). The 0S sample, which does not contain sucrose, undergoes a weight loss of ≈20% between room temperature and 230 °C (Fig. 2d). The corresponding mass spectra show the $m/z = 18$ (H_2O) signal in these temperature ranges. In addition, at ≈150 °C the $m/z = 28$, 30 and 44 signals also are observed in the spectra of the 1S and 0.5S samples but not in the 0S sample (Fig. 2b, d, and f). They are ascribed to N_2, NO and CO_2, respectively. The samples containing sucrose, i.e. the 1S and 0.5S, experience between 150 °C and ≈270 °C another weight loss (≈32% and ≈59%, respectively) being it particularly abrupt for the 0.5S sample (Fig. 2a and c, respectively). The weight loss undergone by the 1S sample is accompanied by a small exothermic effect in the DTA curve at about 250 °C (Fig. 2a) and by a needle-shaped peak in 0.5S sample at almost the same temperature (Fig. 2c). The mass spectra of the 1S and 0.5S samples show in this temperature range signals corresponding to $m/z = 18$, 28, 30 and 44 (Fig. 2b and d). Moreover, the $m/z = 12$ (C) and $m/z = 14$ (N), produced by fragmentation (only shown in Fig. 2b) are also present. The 1S sample shows between 270 °C and 700 °C a new and almost continuous weight loss of ≈28%, but no thermal effects are appreciate in the corresponding DTA curve. The corresponding MS indicates that CO_2 ($m/z = 44$) and N_2/CO ($m/z = 28$) are evolved (Fig. 2b). The signal $m/z = 12$ albeit of low intensity, allows to discriminate between these two molecules, and confirm the evolution of CO in the last part of the thermal treatment. DTA/TG curves of the 0.5S sample do not show any thermal effects between 270 °C and 700 °C that is the final temperature of the analysis (Fig. 2c). For the 0S sample, DTA/TG curves shows between 200 °C and 700 °C a series of endothermic effects and a weight loss of ≈43%. The corresponding MS (Fig. 2f) shows between 200 °C and 450 °C a very intense $m/z = 30$ signal (NO), as well as the $m/z = 32$ (O_2) and 46 (NO_2) (Table 1). It is worth to remark the presence of the $m/z = 32$ (O_2), which has not been observed in the MS spectra of samples 1S and 0.5S. It signifies that some oxygen is formed in the thermal decomposition of the 0S sample, and that for samples 1S and 0.5S, the oxygen from the nitrate decomposition is consumed in the combustion of sucrose.

Differences observed between the thermal behavior of the 1S and 0.5S samples explain the already reported "violent" character of the reaction when the stoichiometric amount of fuel is used in the synthesis [24], i.e. the sample 0.5S. It is worth to remark the needle-shaped exothermic peak in the DTA curve of the 0.5S (Fig. 2c), even working in Ar atmosphere, and the accompanying sudden weight loss observed in the TG curve. Larger amount of sucrose, as in the 1S sample, can reduce the exothermicity of the process. This effect has been observed when some urea fuel is substituted by starch [32].

X-ray diffraction patterns of residues of 1S and 0.5S samples after DTA/TG/MS analysis in Ar are presented in Fig. 1b and c, respectively. They show a group of lines that has been unequivocally ascribed to cubic MnO (78-0424 JCPDS file), as well as a series of low intensity diffraction peaks (marked * and +) that have been assigned to NiC (14-0020 JCPDS file) and to Li_2CO_3 (83-1454 JCPDS file), respectively. To verify that the residues of thermolysis of these two samples in Ar atmosphere kept the correct spinel stoichiometry, they were then heated up to 700 °C in air flow. The recorded TG curves (not shown) indicate a continuous weight increase of ≈11% from room-temperature up to 700 °C, and the X-ray pattern of these residues after thermal treatment in air (Fig. 2d) unequivocally corresponds to a spinel-type compound, with crystallite size of ≈20 nm and lattice parameter $a = 8.1877(8)$ Å, which reasonably agrees with the values reported for $LiNi_{0.5}Mn_{1.5}O_4$, $a = 8.170$ Å (80-2162 JCPDS file). The DRX pattern of the residue of the 0S sample in Ar (Fig. 2e) was indexed in the cubic spinel Fd-3m space group, with $a = 8.297(3)$ Å, being the average crystallite size of ≈30 nm. The lattice parameter is notably larger than that of $LiNi_{0.5}Mn_{1.5}O_4$ (80-2162 JCPDS file). Lattice parameter larger than the reported for stoichiometric $LiMn_2O_4$ based-spinels has been often accounted for based on oxygen defects in the structure [33–35]. The oxygen coming from the nitrate decomposition is not enough to fully oxidize the $Mn(NO_3)_2{\cdot}6H_2O$ reagent, and then not all the Mn cations could be in their maximum oxidation states (Mn^{4+}). Then, to keep the electroneutrality of the obtained spinel oxygen-defects, as well as Mn^{2+} and/or Mn^{3+} must be in the 0S sample. In the pattern shown in Fig. 2e, the (2 2 0) diffraction peak is observed albeit with very low intensity. It indicates the presence of some heavy cations in the 8a tetrahedral sites of the spinel-type structure. Having in mind the preference of Mn^{2+} to situate in the tetrahedral site of the spinel-type structure [36,37], it seems plausible to assume that if a fraction of Mn^{2+} from the thermally decom-

Table 1
TG/DTA/MS data: evolved gaseous products from the 1S, 0.5S, and 0S samples in Ar and in air flow. Sucrose in Ar has been included for comparison.

Molecule	m/z	1S Ar	0.5S Ar	0S Ar	Sucrose Ar	1S air	0.5S air	0S air
C	12	×	×	–	×	×	×	
N	14	×	×	×				
CH_3	15				×			
H_2O	18	×	×	×	×	×	×	×
CO/N_2	28	×	×		×			
NO	30	×	×	×		×	×	×
O_2	32			×				
CO_2	44	×	×		×	×	×	
NO_2	46			×		×	×	×

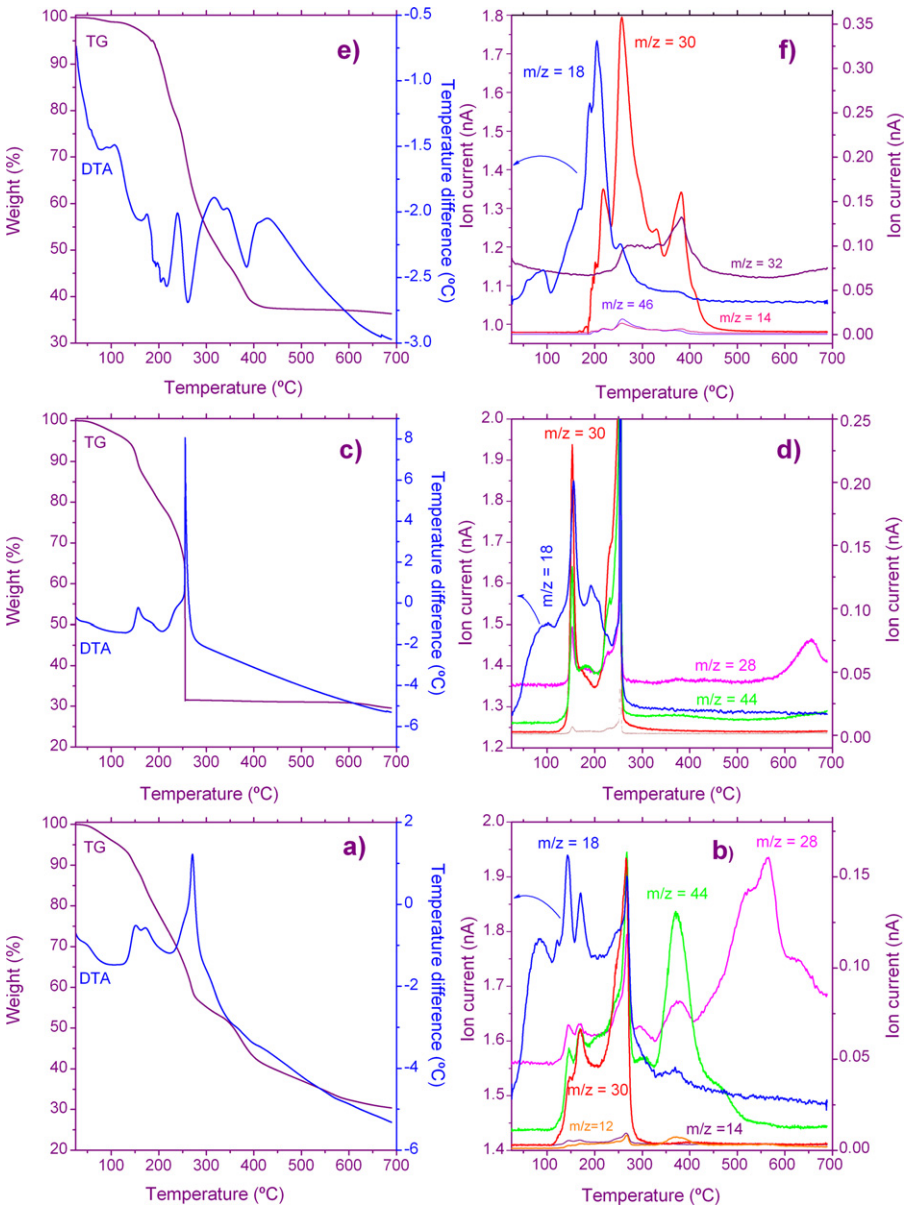

Fig. 2. DTA/TG and MS curves of samples: (a and b) 1S; (c and d) 0.5S and (e and f) 0S recorded in Ar flow.

posed $Mn(NO_3)_2{\cdot}6H_2O$ is not oxidized to Mn^{3+} or Mn^{4+}, it would occupy the tetrahedral 8a position of the Fd-3m space group. The formation of MnO as major component in the decomposition products of 1S and 0.5S reagents instead of spinel, reveals that oxygen from the nitrate decomposition is more strongly concerned in combustion of sucrose than in oxidation of Mn^{2+} from the $Mn(NO_3)_2$ reagent.

TG/DTA/MS curves recorded in air flow are presented in Fig. 3. For the 0.5S and 1S samples three exothermic effects are observed up to 350 °C (about 150 °C, 260 °C and 330 °C). The two first effects are more intense for 0.5S than for 1S sample. However the thermal process at ≈330 °C is more exothermic for the latter and the weight loss undergone by the 0.5S (64.8%) is smaller than for the 0.5S (73.4%) (Table 2). For the 0S sample, the DTA curve recorded in air flow (Fig. 3e) does not show exothermic peaks being it quite similar to the one recorded in Ar flow (Fig. 2e). The total weight loss observed in the TG curve in air is also very close to the value determined for this sample in Ar, 62.7% and 63.7%, respectively (Table 2).

Mass spectra recorded for sample 0.5S and 1S (Fig. 3b and d) show the m/z = 18, 30, 44, and 46 signals, being them ascribed to H_2O, NO, CO_2 and NO_2, respectively. For the two first exothermic processes CO_2, H_2O and NO are observed in the MS. This result indicates that the combustion of sucrose and nitrate decomposition is taking place simultaneously. During the exothermic process at ≈330 °C the MS of the 0.5S sample (Fig. 3d) shows a broad signal of CO_2. However, for the 1S sample CO_2 and H_2O signals are observed during this thermal process. This later result is ascribed to the combustion of sucrose excess in the 1S sample, and it explains the higher weight loss observed for this sample. Mass spectrum recorded for the 0S sample (Fig. 3f) only shows signals m/z = 18, 30 and 46. Gases identified in the MS spectra of the samples 1S, 0.5S and 0S in Ar and in air flow are summarized in Table 1.

XRD patterns of the residues from TG/DTA/MS analysis in air are shown in Fig. 4a–c. They correspond to the $LiNi_{0.5}Mn_{1.5}O_4$ spinel, and all of them have almost the same lattice parameter ($a \approx 8.173$ Å) which is in excellent agreement with the one reported for this cubic Fd-3m spinel ($a = 8.170$ Å, 80-2162 JCPDS file). Now, in these

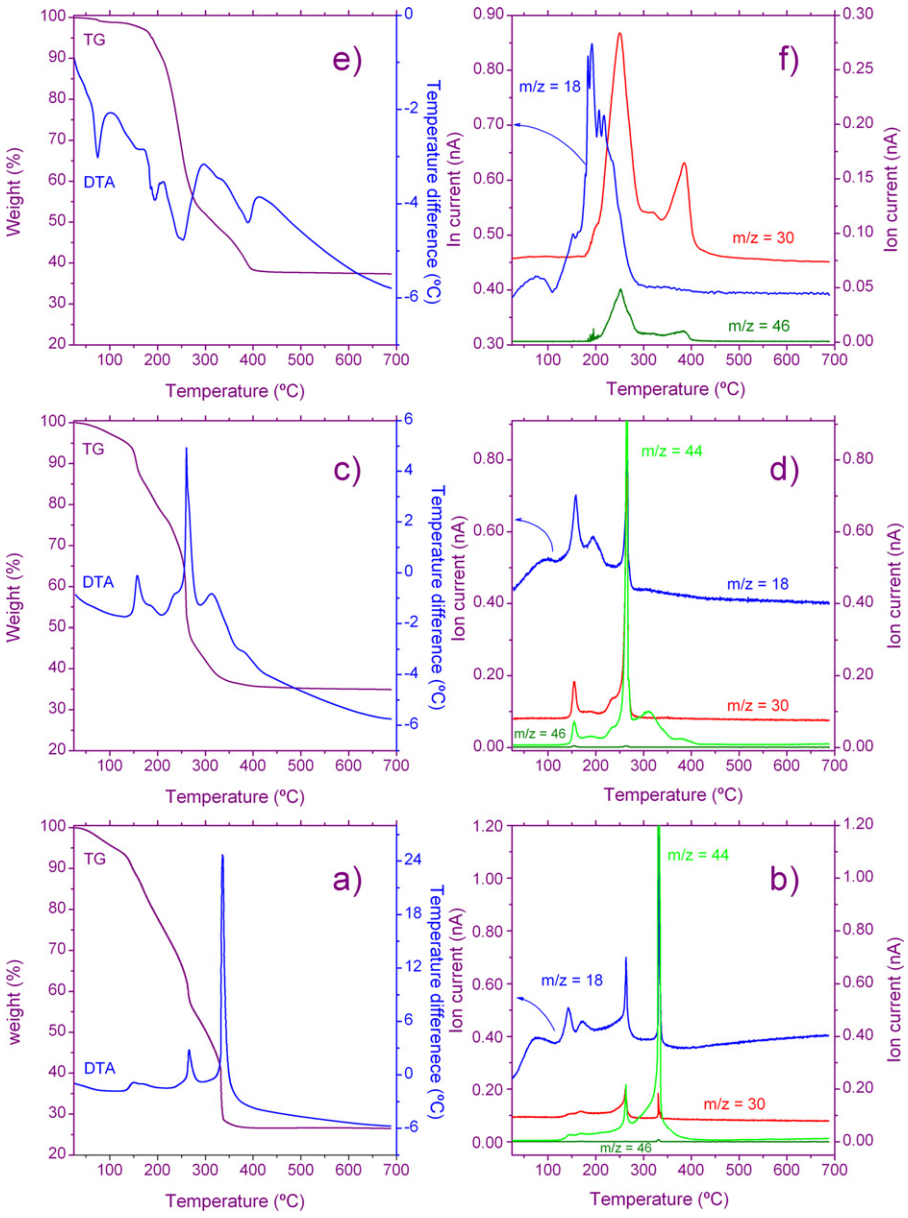

Fig. 3. DTA/TG and MS curves of samples: (a and b) 1S; (c and d) 0.5S and (e and f) 0S recorded in air flow.

patterns, the (2 2 0) diffraction peak is not observed. The average crystallite size of the residues obtained for 1S and 0.5S samples after the thermal treatment in air was ≈40 nm, while the size determined for the residue of the 0S sample was ≈30 nm. This value is identical to the one determined for the spinel-type compound obtained from thermal decomposition of sample 0S in Ar flow (≈30 nm), and it is slightly smaller than the ones determined for the spinel obtained from the thermal treatment in air. This result can be explained if we compare DTA curves shown in Fig. 3a and c with the DTA curves shown in Figs. 2e and 3e. These two latter are quite similar, and no exothermic peaks are observed either in Ar (Fig. 2e) or in air flow (Fig. 3e). However, exothermic effects are present in the DTA curves of the 1S and 0.5S in air (Fig. 3a and c). The local increase of temperature can account for the slightly larger average crystallite size determined for the spinels formed in air flow, even though it is always very small as is commonly observed for compounds synthesized by the sucrose-aided combustion procedure.

From the results obtained by X-ray diffraction and TG/DTA/MS it comes out that the equation proposed in Eq. (1) can now be completed. The reactions undergo by the mixture of oxidant (nitrates)

Table 2
Overall experimental and calculated weight losses for the 1S, 0.5S and 0S in argon and in air flow. The weight losses have been calculated from Eq. (2)–(7). Theoretical weight losses have been calculated assuming the anhydrous reagents.

1S				0.5S				0S			
Ar		Air		Ar		Air		Ar		Air	
Calc. (%)	Exp. (%)	Calc. (%)	Exp. (%)	Calc. (%)	Exp. (%)	Calc. (%)	Exp. (%)	Calc. (%)	Exp. (%)	Calc. (%)	Exp. (%)
69	69.2	76.3	73.4	70.2	70.4	69.6	64.8	57.4	62.5	57.4	62.3

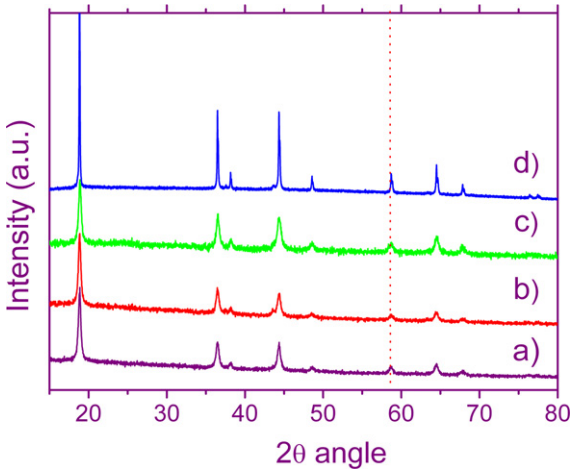

Fig. 4. X-ray diffraction patterns of DTA/TG/MS residues in air flow of samples: (a) 1S; (b) 0.5S and (c) 0S; (d) 0S-700N800A (obtained from the 0S sample heated in N_2 at 700 °C and then in air at 800 °C).

and fuel (sucrose) in an inert atmosphere (Ar) could be as follows:

$$LiNO_3 + 0.5Ni(NO_3)_2 + 1.5Mn(NO_3)_2 + C_{12}H_{22}O_{11} \rightarrow 1.5MnO + 0.5NiC + 0.5Li_2CO_3 + 11H_2O + 5NO + 4CO + 2CO_2 + 5C \quad (2)$$

$$LiNO_3 + 0.5Ni(NO_3)_2 + 1.5Mn(NO_3)_2 + 0.5C_{12}H_{22}O_{11} \rightarrow 1.5MnO + 0.5NiC + 0.5Li_2CO_3 + 5.5H_2O + 5NO + 2CO + 3CO_2 \quad (3)$$

$$LiNO_3 + 0.5Ni(NO_3)_2 + 1.5Mn(NO_3)_2 \rightarrow LiNi_{0.5}Mn_{1.5}O_{4-\delta} + 4NO + NO_2 + 2O_2 + (nH_2O) \quad (4)$$

Eqs. (2)–(4) would apply for the 1S, 0.5S and 0S samples, respectively. When the reaction is carried out in air flow, the following equations are proposed:

$$LiNO_3 + 0.5Ni(NO_3)_2 + 1.5Mn(NO_3)_2 + C_{12}H_{22}O_{11} \xrightarrow{+9.5O_2} LiNi_{0.5}Mn_{1.5}O_4 + 11H_2O + 4NO + NO_2 + 12CO_2 \quad (5)$$

$$LiNO_3 + 0.5Ni(NO_3)_2 + 1.5Mn(NO_3)_2 + 0.5C_{12}H_{22}O_{11} \xrightarrow{+3.5O_2} LiNi_{0.5}Mn_{1.5}O_4 + 5.5H_2O + 4NO + NO_2 + 6CO_2 \quad (6)$$

$$LiNO_3 + 0.5Ni(NO_3)_2 + 1.5Mn(NO_3)_2 \xrightarrow{+2O_2} LiNi_{0.5}Mn_{1.5}O_4 + 3NO + 2NO_2 + (nH_2O) \quad (7)$$

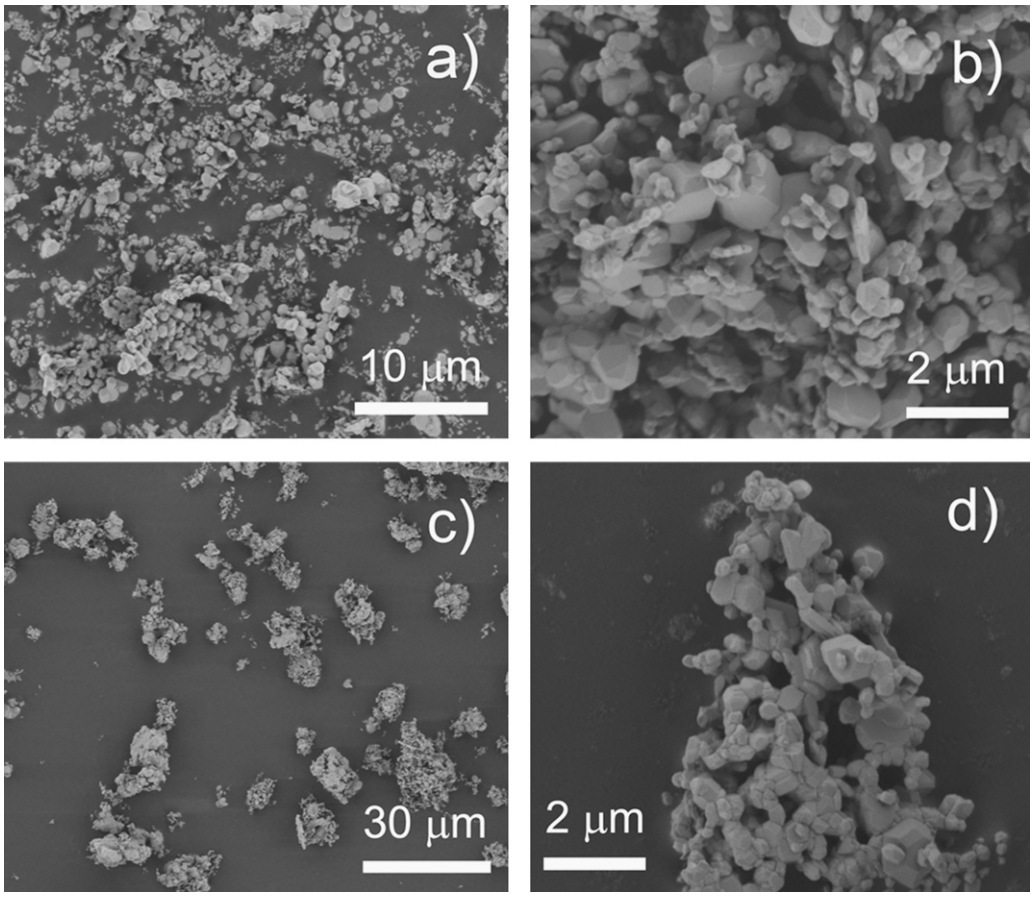

Fig. 5. FE-SEM micrographs of the: (a and b) LNMS obtained after thermal treatment of the 1S sample at 800 °C 4 h in air (1S-800A); (c and d) LNMS obtained after thermal treatment of the 0S sample at 700 °C 4 h in N_2 and at 800 °C 4 h in air (0S-700N800A).

Eqs. (5)–(7) would apply for the 1S, 0.5S and 0S samples, respectively. Results shown in Table 2 indicate that the agreement between the calculated from the proposed equations and the experimental weight loss is good for the 1S and 0.5S samples, and only small discrepancies occur for 0S both in Ar and in air flow.

3.2. Electrochemical studies

It has been before mentioned that cathode composites containing $LiNi_{0.5}Mn_{1.5}O_4$ as active material are the ones among the family of the $LiMn_2O_4$–based spinels, able to accumulate largest amount of energy [24–30]. Thus, we have considered worthwhile to study the electrochemical properties of the LNMS spinels obtained as residues after the TG/DTA/MS studies. To do that, ≈1 g of several LNMS spinels were synthesized following the synthesis conditions indicated in Section 2. The corresponding XRD patterns indicate that they are all single phase spinels, being their lattice parameters summarized in Table 3. The lattice parameter of the 0S-700N sample synthesized in N_2 (a = 8.2409(9) Å) is slightly smaller than the one determined for the spinel obtained from the TG/DTA/MS in Ar, but larger than the usually reported for $LiNi_{0.5}Mn_{1.5}O_4$. The pattern also shows the (2 2 0) reflection as a low intensity peak. The crystallite size determined for 0S-700N (≈28 nm) is practically identical to the one determined for the residue obtained from TG/DTA/MS. All these results show that the LNMS samples synthesized are similar to those obtained in the TG/DTA/MS study. For the 0S-700N800A, 0S-800A and 1S-800A samples the doublet $K\alpha_1,\alpha_2$ observed for the diffraction peaks $2\theta \geq 40^\circ$ is symptomatic of very high crystalline samples. As an example, the XRD of 0S-700N800A is shown in Fig. 4d. The FWHM of the XRD lines is nearly the same as that of the standard, so the crystallite size cannot be correctly estimated from the Scherrer equation. Thus, the particle size was investigated by FE-SEM. Micrographs of the 1S-800A and 0S-700N800A samples are shown in Fig. 5. It can be observed that the 1S-800A spinel has a morphology consisting of very crystalline discrete particles (Fig. 5a) with well developed faces (Fig. 5b). The average particle size determined from the FE-SEM micrographs is 0.46 μm although some heterogeneity is observed. FE-SEM images of the 0S-700N800A spinel show a very different morphology. The sample consists of aggregates of small and homogeneous particles with well defined faces that are assembled together. They form porous isolated clusters (Fig. 5c) of primary crystalline submicrometric particles leaving some porosity among them. The primary particles are more homogeneous than that of the 1S-800A sample but close in size, being the average size 0.5 μm (Fig. 5d). The FE-SEM studies show that when sucrose is used in the synthesis the liberation of large volume of gaseous products avoids the assemblage of the particles, and the nanostructuration in the cluster of the sample.

In Fig. 6 the charge/discharge curves corresponding to the cycles in which the LNMSs samples furnish their maximum discharge capacity are shown. In all cases, charge/discharge curves exhibit two plateaus, one at very high potential in the 4.7 V region, and the other is in the 4 V region. For the 0S-800A and 1S-800A samples, both synthesized in air, the capacity furnished in the 4.7 V plateau is much higher than the one delivered in the 4 V plateau ($Q_{4.7\,V} \approx 100$ mAh g^{-1} and $Q_{4\,V} \approx 10$ mAh g^{-1}, respectively). The large plateau at 4.7 V has been ascribed to the two-steps (Ni^{4+}/Ni^{3+}, Ni^{3+}/Ni^{2+}) redox reactions [35,38,39]. The small plateau at ≈4 V, which is observed in most of the LNMS-based cathodes, is due to the presence of residual amount of Mn^{3+} in the spinel [34,35,39,40]. The maximum discharge capacity (Q_{max}) determined at the end of the reduction curves (Fig. 6) as well as the cycle for which Q_{max} is reached, have been summarized in Table 3. The capacity values are comparable to the ones reported

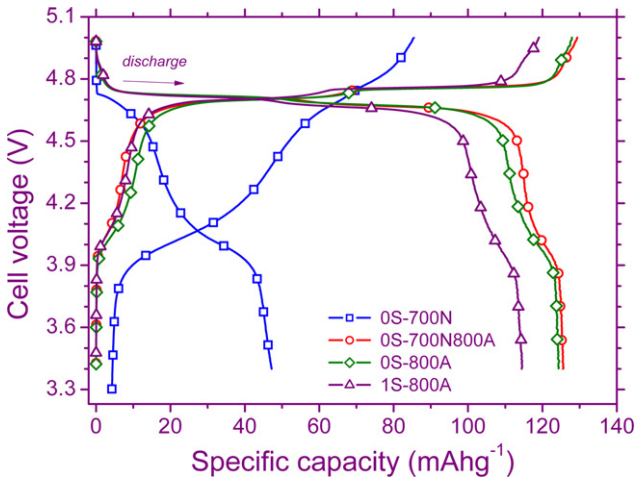

Fig. 6. Charge/discharge curves for the LNMSs: 0S-700N; 0S-700N800A; 0S-800A and 1S-800A recorded at 25 °C. Curves correspond to the cycle for which the maximum discharge capacity was reached.

for LNMS-samples obtained using different synthesis procedures [26,27,29,41,42].

For the 0S-700N spinel, the only one synthesized in inert atmosphere, the charge/discharge capacities (Q_{ch} = 85.4 mAh g^{-1}, Q_{dch} = 47.2 mAh g^{-1}) are significantly lower than the ones measured for the samples synthesized in air (Table 3). Moreover, the specific capacities in the 4 V region (Q_{ch} = 48 mAh g^{-1}, Q_{dch} = 29.2 mAh g^{-1}) are higher than those in the 4.7 V region (Q_{ch} = 37.4 mAh g^{-1}, Q_{dch} = 18 mAh g^{-1}). The increase of $Q_{4\,V}$ compared to the one observed for the samples synthesized in air indicates that the 0S-700N sample has higher Mn^{3+} content. It can be accounted for by the oxygen deficiency of this sample deduced from by XRD data, i.e. the large lattice parameter value of this sample (Table 3). The modest capacity of 0S-700N can be justified by both the oxygen defects and by the presence of heavy atoms in the 8a sites of the Fd-3m structure, as shown by the (2 2 0) diffraction peak observed in the XRD pattern. The heavy atoms placed in tetrahedral sites difficult the mobility of the Li^+ through the three-dimensional channels of the spinel structure. These explanations have also been put forward by Pasero et al. [34] and by Hagh et al. [37] to justify the lower capacity delivered by LNMS samples with oxygen defects or with heavy cations in 8a tetrahedral positions, respectively.

Having in mind previous TG/DTA results which showed that the spinel obtained from the 0S sample heated in inert atmosphere undergone a weight increase when it is heated in air, we thought it was possible to improve the capacity of the 0S-700N sample by heating it for 4 h in air at 800 °C (0S-700N800A sample). The lattice parameter determined for 0S-700N800A, a = 8.1675(3) Å, is smaller than that of 0S-700N, a = 8.2409(9) Å. This result is consistent with the increase in oxidation state of manganese cations to Mn^{4+} on removing the oxygen defects. The lattice parameter of the 0S-700N800A is in excellent agreement with the one reported for $LiNi_{0.5}Mn_{1.5}O_4$ and with the ones determined for the 0S-800A and 1S-800A samples synthesized in air (Table 3). Moreover, the XRD pattern of the sample 0S-700N800A does not show now the (2 2 0) diffraction peak observed for the 0S-700N, indicating that the heavy atoms in the 8a tetrahedral sites are shifted towards the 16d octahedral position in the Fd-3m structure. The charge/discharge curves recorded for the 0S-700N800A (Fig. 6) are similar to the ones obtained for the 0S-800A and 1S-800A, being the capacity the largest of all the samples studied (Q_{max} = 126 mAh g^{-1}). Now, the capacity of the 4 V region is significantly lower than the one shown by the 0S-700N sample indicating that the Mn^{3+} content has

Table 3
Thermal treatment, lattice parameter, maximum discharge capacity (Q_{max}) and corresponding cycle number, capacity retention after 50 cycles (QRt-50) and normalized capacity loss by cycle for the 0S-700N, 0S-700N800A, 0S-800A, and 1S-800A spinels. Electrochemical performances of 0S-700N800A at 55 °C have also been included.

Sample	Thermal treatment	Lattice parameter (Å)	Q_{max} (mAh g^{-1})	Cycle number for Q_{max}	QRt-50 (%)	Capacity loss by cycle (%)
0S-700N	700 °C, 4 h, N_2	8.2404(9)	47.2	1	96.84	0.0194
0S-700N800A	0S-700N +800 °C	8.1675(3)	126	5	97.55	0.0557
0S-700N800A at 55 °C	4 h, air	8.1675(3)	123	3	95.62	0.0967
0S-800A	800 °C, 4 h, air	8.169(2)	124	4	97.0	0.06
1S-800A	800 °C, 4 h, air	8.1663(4)	115	3	94.1	0.1161

decreased and hence, the oxygen defects on heating in air. Moreover, the remarkable improvement in the electrochemical response is also accounted for by the migration of the heavy cations to the 16d octahedral positions. The electrochemical results confirm that the spinel-type compound formed at 700 °C in inert atmosphere has the right cations stoichiometry, but it is oxygen deficient. It only requires further thermal treatment in air to yield $LiNi_{0.5}Mn_{1.5}O_4$ able to be used as cathode material in Li-ion batteries.

The cycling behavior of the synthesized LNMSs has been studied at 0.2*C* charge/discharge rate in the potential range from 3.4 to 5.2 V. As an example, a selection of charge/discharge curves recorded during the cycling of the 0S-700N800A sample is plotted in Fig. 7a. All curves are very similar, showing the large plateau with two steps in the 4.7 V region and the small plateau at ≈4 V. The likeness of the redox voltages for the different cycles indicates that the cell polarization remain roughly unchanged on cycling. For every cycle, the charge capacity is slightly higher than the discharge one indicating that some oxidation of the electrolyte takes place at the end of the charge step. The coulombic efficiency ($Q_{dch} \times 100/Q_{ch}$) determined for 0S-700N800A is 96.8% in average during cycling, being it higher for the other LNMS samples studies (98.1% for 0S-800A and 99.1% for 1S-800A). In the inset of Fig. 7a, the Nyquist plots recorded after the 20th and 50th cycles for the Li//0S-700N800A cell are compared. It is observed that, in spite of the electrolyte degradation, the cell impedance does not significantly increase on cycling, being it ≈11 Ω. In fact, the discharge capacity only decreases from Q_{max} = 126 mAh g^{-1} (5th cycle) to 122.5 mAh g^{-1} for the 50th cycle; the capacity retention after 50 cycles is QRt-50 = 97.55%. This high value points out the remarkable cyclability of the 0S-700N800A spinel. In Fig. 7b the evolution of discharge capacity vs. cycle number at 25 °C for synthesized LNMS-spinels is plotted. For every sample a very small and almost linear diminution of Q_{dch} is observed. From the slope determined by linear fitting, the normalized capacity loss by cycle in percent was calculated according to the expression: slope × 100/Q_{max}. The corresponding values are summarized in Table 3 together with QRt-50. In all cases, the capacity retention is higher than 90% showing the remarkable cycling performances of all the synthesized spinels. Among them, 0S-700N800A shows the highest QRt-50 value (97.55%) being its capacity loss by cycle of only 0.0557%. It is worth to remark that this cycling performance is among the best reported in the literature for LNMS-based cathodes [26,27,29,41–44].

It is well known that the main drawback of the LNMS-based cathodes is the severe capacity loss when cycling is carried out at elevated temperature (≈55 °C) [27,29,35,37,43]. Thus, we have decided to study the cycling behavior of the 0S-700N800A sample at 55 °C and in Fig. 7b the evolution of Q_{dch} vs. cycle number is plotted. Measurements were also carried out at 0.2*C* ch/dch rate in the potential range from 3.4 V to 5 V. As for 25 °C, a very small and almost linear diminution of Q_{dch} on cycling is observed. Their QRt-50 value is high (95.62%) being the normalized capacity loss by cycle of only 0.0967%. These values, which are close to those obtained at 25 °C (Table 3) illustrates the notable cycling performances of the 0S-700N800A spinel even at elevated temperature. These remarkable electrochemical properties could be explained by the high crystallinity of the sample, as it was shown by XRD and FE-SEM studies, together with a well-suited morphology. The occurrence of porous clusters of submicrometric primary particles (Fig. 5c and d) allows the electrolyte contacts with the individual particles and their aggregation seems to increase the stability of the sample against the electrolyte even at elevated temperature.

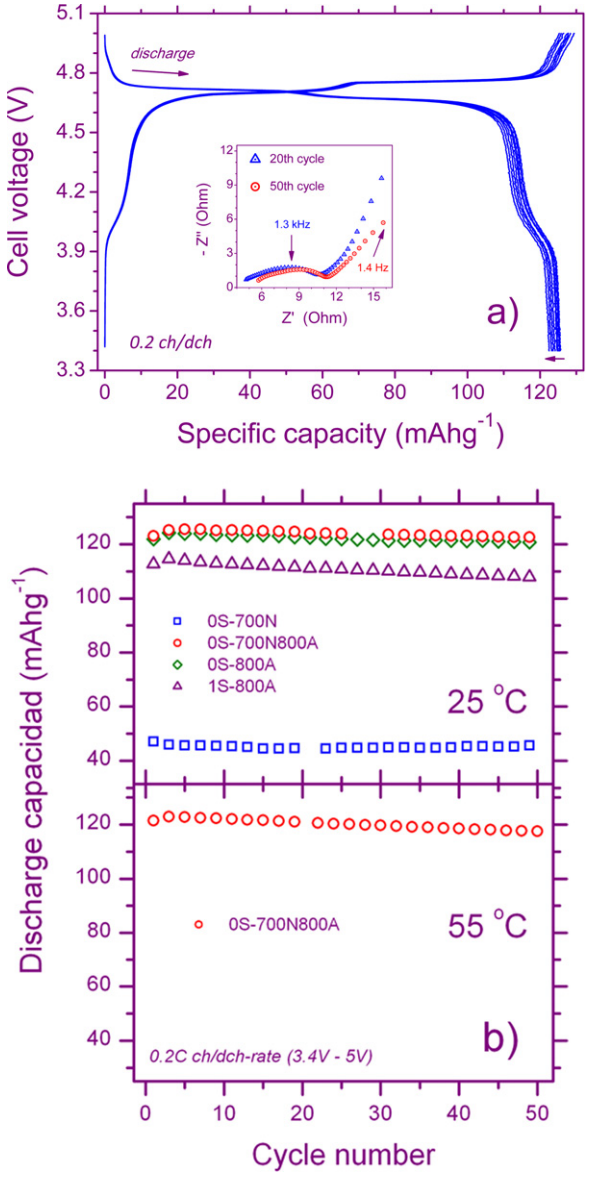

Fig. 7. (a) Selection of charge/discharge curves recorded during the cycling of 0S-700N800A at 25 °C. The inset shows the Nyquist plots of the cell after the 20th and 50th cycles. (b) Evolution of discharge capacity vs. cycle number at 25 °C for 0S-700N; 0S-700N800A; 0S-800A and 1S-800A spinels. For 0S-700N800A, evolution at 55 °C is also plotted. (Cycling studies were performed at 0.2*C* charge/discharge rate in the potential range from 3.4 to 5 V.)

4. Conclusions

Thermal (TG/TA/MS) studies have allowed identification of the gases evolved along heating of metal nitrate reagents with and without sucrose as fuel both in air and in Ar. It allows us to propose the equations for the sucrose-assisted LCS process. In air atmosphere, sub-micrometric LNMS samples are obtained regardless the amount of sucrose used in the synthesis. The fuel amount modifies the morphology of the samples. When sucrose is used the sample consists of discrete particles, but microcrystalline clusters of primary particles are obtained from the nitrate mixture without sucrose. In inert atmosphere a spinel-type compound is only attained when the mixture of reagents are thermally treated without sucrose. It is an oxygen-deficient spinel with heavy atoms in the tetrahedral sites. When sucrose is added, the oxygen generated in the decomposition of nitrates preferentially reacts with the sucrose avoiding the oxidation of Mn^{2+}, and hence, the formation of the spinel. In all cases, a further thermal treatment in air yields analogous LNMSs which are also similar to the ones obtained when the mixture of nitrates are directly treated in air.

The studies of the electrochemical properties of synthesized LNMSs show that they heavily depend on the atmosphere of synthesis. Thus, the spinel prepared in inert atmosphere, although it has an excellent cyclability (QRt-50 = 96.84%), its capacity is small ($47.2\ mAh\ g^{-1}$). This low *Q*-value has been attributed to the presence of oxygen defects and heavy atoms in tetrahedral sites. When this defective sample is heated in air, its capacity remarkably increases up to $126\ mAh\ g^{-1}$. This value is similar to the ones shown by the LNMSs directly synthesized in air, and comparable to the best reported in the literature. Moreover, all these samples have a very high voltage ($\approx$4.7 V), elevated specific energy ($\approx 565\ mWh\ g^{-1}$) and high cyclability (QRt-50 > 90%) even at elevated temperature (55 °C). These remarkable electrochemical performances show that the synthesized samples are very promising cathode material especially for practical Li-ion battery required for hybrid and electrical vehicles.

Acknowledgements

Financial support through the projects MAT2008-03182 (MICINN), MATERYENER P2009/PPQ-1626 (CAM) and 2009MA0007 (CSIC/CNRST) is gratefully recognized.

References

[1] S.S. Manoharan, N.R.S. Kumar, K.C. Patil, Mater. Res. Bull. 25 (1990) 731–738.
[2] K. Suresh, N.R.S. Kumar, K.C. Patil, Adv. Mater. 3 (1991) 148–150.
[3] N.A. Dhas, K.C. Patil, J. Solid State Chem. 102 (1993) 440–445.
[4] S.T. Aruna, A.S. Mukasyan, Curr. Opin. Solid State Mater. Sci. 12 (2008) 44–50.
[5] R. Ianoş, I. Lazău, C. Păcurariu, P. Barvinschi, Mater. Res. Bull. 43 (2008) 3408–3415.
[6] P.P. Sarangi, B. Naik, N.N. Ghosh, Powder Technol. 192 (2009) 245–249.
[7] X.-H. Huang, J. Chang, Mater. Chem. Phys. 115 (2009) 1–4.
[8] Md.H. Zahir, T. Suzuki, Y. Fujishiro, Ma. Awano, Appl. Catal. A 361 (2009) 86–92.
[9] S.V. Chavan, P.U.M. Sastry, A.K. Tyagi, J. Alloys Compd. 456 (2008) 51–56.
[10] X. Mi, X. Zhang, X. Ba, Z. Bai, L. Lu, Xi. Wang, Q. Liu, Adv. Powder Technol. 20 (2009) 164–168.
[11] R.P. Sonekar, S.K. Omanwar, S.V. Moharil, P.L. Muthal, S.M. Dhopte, V.K. Kond, J. Lumin. 129 (2009) 624–628.
[12] E.C. Fuchs, C. Sommer, F.P. Wenzl, B. Bitschnau, A.H. Paulitsch, A. Mühlanger, K. Gatterer, Mater. Sci. Eng. B 156 (2009) 73–78.
[13] A.S. Aricò, P. Bruce, B. Scrosati, J.M. Tarascon, W. Van Schalkwijk, Nat. Mater. 4 (2005) 366–377.
[14] J.B. Goodenough, Y. Kim, Chem. Mater. 22 (2010) 587–603.
[15] S.B. Yi, H.T. Chung, H.G. Kim, Electrochem. Commun. 9 (2007) 591–595.
[16] M. Dahbi, I. Saadoune, J.M. Amarilla, Electrochim. Acta 53 (2008) 5266–5271.
[17] O. Haik, S.K. Martha, H. Sclar, Z. Samuk-Fromovich, E. Zinigrad, B. Markovsky, D. Kovacheva, N. Saliyski, D. Aurbach, Thermochim. Acta 493 (2009) 96–104.
[18] A.S. Prakash, P. Manikandan, K. Ramesha, M. Sathiya, J.M. Tarascon, A.K. Shukla, Chem. Mater. 22 (2010) 2857–2863.
[19] D. Kovacheva, H. Gadjov, K. Petrov, S. Mandal, M.G. Lazarraga, L. Pascual, J.M. Amarilla, R.M. Rojas, P. Herrero, J.M. Rojo, J. Mater. Chem. 12 (2002) 1184–1188.
[20] M.S. Whittingham, Chem. Rev. 104 (2004) 4271–4301.
[21] J.M. Amarilla, R.M. Rojas, F. Picó, L. Pascual, K. Petrov, D. Kovacheva, M.G. Lazarraga, I. Lejona, J.M. Rojo, J. Power Sources 174 (2007) 1212–1217.
[22] B.L. Ellis, K.T. Lee, L.F. Nazar, Chem. Mater. 22 (2010) 691–714.
[23] J.M. Amarilla, K. Petrov, F. Picó, G. Avdeev, J.M. Rojo, R.M. Rojas, J. Power Sources 191 (2009) 591–600.
[24] M.G. Lazarraga, L. Pascual, H. Gadjov, K. Petrov, J.M. Amarilla, R.M. Rojas, M.A. Martín-Luengo, J.M. Rojo, J. Mater. Chem. 14 (2004) 1640–1647.
[25] R. Alcántara, M. Jaraba, P. Lavela, J.L. Tirado, J. Electroanal. Chem. 566 (2004) 187–192.
[26] K.M. Shaju, P.G. Bruce, Dalton Trans. (2008) 5471–5475.
[27] S. Patoux, L. Sannier, H. Lignier, Y. Reynier, C. Bourbon, S. Jouanneau, F. Le Cras, S. Martinet, Electrochim. Acta 53 (2008) 4137–4145.
[28] M. Aklalouch, J.M. Amarilla, R.M. Rojas, I. Saadoune, J.M. Rojo, Electrochem. Commun. 12 (2010) 548–552.
[29] R. Santhanam, B. Rambabu, J. Power Sources 195 (2010) 5442–5451.
[30] Q. Zhong, A. Bonakdarpour, M. Zhang, Y. Gao, J.R. Dahn, J. Electrochem. Soc. 144 (1997) 205–213.
[31] J. Laugier, A. Filhol, CelRef, PC version CELREF program, ILL, Grenoble, France, 1991 (unpublished).
[32] K. Tahmasebi, M.H. Paydar, Mater. Chem. Phys. 109 (2008) 156–163.
[33] P. Strobel, A. Ibarra Palos, M. Anne, J. Power Sources 97–98 (2001) 381–384.
[34] D. Pasero, N. Reeves, V. Pralong, A.R. West, J. Electrochem. Soc. 155 (2008) A282–A291.
[35] M. Aklalouch, R.M. Rojas, J.M. Rojo, I. Saadoune, J.M. Amarilla, Electrochim. Acta 54 (2009) 7542–7550.
[36] T. Yokoyama, Y. Abe, T. Meguro, K. Komeya, K. Kondo, S. Kanebo, T. Sasamoto, Jpn. J. Appl. Phys. 3 (1996) 5775–5780.
[37] N.M. Hagh, G.G. Amatucci, J. Power Sources 195 (2010) 5005–5012.
[38] Y. Terada, K. Yasaka, F. Nishikawa, T. Konishi, M. Yoshio, I. Nakai, J. Solid State Chem. 156 (2001) 286–291.
[39] M. Kunduraci, G.G. Amatucci, J. Power Sources 165 (2007) 359–367.
[40] J.H. Kim, S.T. Myung, C.S. Yoon, S.G. Kang, Y.K. Sun, Chem. Mater. 16 (2004) 906–914.
[41] J.C. Arrebola, A. Caballero, L. Hernán, J. Morales, J. Power Sources 183 (2008) 310–315.
[42] M. Aklalouch, J.M. Amarilla, R.M. Rojas, I. Saadoune, J.M. Rojo, J. Power Sources 185 (2008) 501–511.
[43] Y.K. Sun, Lee, M. Yoshio, K. Amine, Electrochem. Solid-State Lett. 5 (2002) A99–A102.
[44] R.M. Rojas, J.M. Amarilla, L. Pascual, J.M. Rojo, D. Kovacheva, K. Petrov, J. Power Sources 160 (2006) 529–535.